



Non-linear Dose Response of Lymphocyte Cell Lines to Microtubule Inhibitors

Daria M. Potashnikova^{1,2*}, Aleena A. Saidova^{1,3}, Anna V. Tvorogova^{3,4}, Eugene V. Sheval⁴ and Ivan A. Vorobjev^{1,4,5}

¹ Department of Cell Biology and Histology, School of Biology, M.V. Lomonosov Moscow State University, Moscow, Russia, ² Laboratory of Atherothrombosis, Moscow State University of Medicine and Dentistry, Moscow, Russia, ³ Department of Cell Biotechnology, Center of Experimental Embryology and Reproductive Biotechnology, Moscow, Russia, ⁴ A.N. Belozersky Institute of Physico-Chemical Biology, M.V. Lomonosov Moscow State University, Moscow, Russia, ⁵ Department of Biology, School of Science and Technology, Nazarbayev University, Astana, Kazakhstan

OPEN ACCESS

Edited by:

Vadim V. Sumbayev,
University of Kent, United Kingdom

Reviewed by:

Martin Degen,
Universität Bern, Switzerland
John Holmes Miller,
Victoria University of Wellington,
New Zealand

*Correspondence:

Daria M. Potashnikova
dpotashnikova@gmail.com

Specialty section:

This article was submitted to
Experimental Pharmacology
and Drug Discovery,
a section of the journal
Frontiers in Pharmacology

Received: 08 February 2019

Accepted: 05 April 2019

Published: 24 April 2019

Citation:

Potashnikova DM, Saidova AA,
Tvorogova AV, Sheval EV and
Vorobjev IA (2019) Non-linear Dose
Response of Lymphocyte Cell Lines
to Microtubule Inhibitors.
Front. Pharmacol. 10:436.
doi: 10.3389/fphar.2019.00436

Microtubule (MT) inhibitors show anti-cancer activity in a wide range of tumors *in vitro* and demonstrate high clinical efficacy. To date they are routinely included into many chemotherapeutic regimens. While the mechanisms of MT inhibitors' interactions with tubulin have been well-established, the relationship between their concentration and effect on neoplastic cells is not completely understood. The common notion is that tumor cells are most vulnerable during division and all MT inhibitors block them in mitosis and induce mitotic checkpoint-associated cell death. At the same time multiple evidence of more subtle effects of lower doses of MT inhibitors on cell physiology exist. The extent of efficacy of the low-dose MT inhibitor treatment and the mechanisms of resulting cell death currently present a critical issue in oncology. The prospect of MT inhibitor dose reduction is promising as protocols at higher concentration have multiple side effects. We assessed cell cycle changes and cell death induced by MT inhibitors (paclitaxel, nocodazole, and vinorelbine) on human lymphoid B-cell lines in a broad concentration range. All inhibitors had similar accumulation effects and demonstrated "trigger" concentrations that induce cell accumulation in G2/M phase. Concentrations slightly below the "trigger" promoted cell accumulation in sub-G1 phase. Multi-label analysis of live cells showed that the sub-G1 population is heterogeneous and may include cells that are still viable after 24 h of treatment. Effects observed were similar for cells expressing Tat-protein. Thus cell cycle progression and cell death are differentially affected by high and low MT inhibitor concentrations.

Keywords: cell cycle, cell death, microtubule inhibitors, paclitaxel, nocodazole, vinorelbine, B-lymphocytes, RPMI8866

INTRODUCTION

The importance of microtubule (MT) dynamics for cell motility (Liao et al., 1995), migration (Kaverina and Straube, 2011), and division (Jordan et al., 1993) has been well-established. The multi-aspect effect of suppressed microtubule dynamics makes MT inhibitors an important part of most anti-cancer chemotherapeutic regimens by inhibiting tumor growth (antimitotic effect) and metastasis (antimigration effect) (Dumontet and Jordan, 2010).

Microtubule inhibitors encompass several classes of compounds with varying mechanisms of interactions with tubulin (Perez, 2009) that disrupt MT dynamics by either stabilizing or de-stabilizing them. MT inhibitors of the first generation widely used in clinics (taxanes, vinca alkaloid derivatives) have certain drawbacks, including neurotoxic effects (Windebank, 1999), neutropenia (Donehower and Rowinsky, 1993) and loss of efficacy against advanced forms of some cancers (Sève et al., 2008). Clinical limitations in treatment of solid tumors and hematologic malignancies prompted further research for analogs with improved clinical characteristics, recently introducing vinflunine, epothilones, indibulin, and many other (Bennouna et al., 2008; Cortes and Vidal, 2012).

Varying effects of high and low MT inhibitor concentrations on different aspects of cell physiology have been described for a number of cell models (Grigoriev et al., 1999; Yang et al., 2010). The first meta-analysis focused on efficacy and toxicity of low-dose versus conventional-dose chemotherapies has been published recently (Xie et al., 2017) and provided data on low-dose chemotherapy advantages.

Microtubule inhibitors are integrated into a variety of chemotherapy schemes for B-cell malignancies, including the curative regimens of non-Hodgkin lymphomas (Bates et al., 2016). Their anti-cancer effects extend beyond their ability arrest mitosis and include their potential to induce apoptosis at all cell cycle phases (Bates and Eastman, 2017). The physiological consequences of MT dynamics inhibition are still poorly understood; the elucidation of its pleiotropic effects on cell death and cell cycle will provide novel therapeutic strategies. In this study we sought to determine the lowest efficient concentration of several MT inhibitors and tested their dose-dependent effects on cell death and mitotic arrest on B-cell lines RPMI8866 and its Tat-expressing modification RPMI8866-Tat-GFP. B-cell lymphomas (Burkitt lymphoma, DLBCL, and B-CLL) are one of the most common comorbid conditions for HIV-infected patients (Gopal et al., 2013). B-cell oncogenesis in HIV patients is related to Tat viral protein that enters B-lymphocytes, acts as a transcription factor in oncogenic cascades (Vendrame et al., 2014; Musinova et al., 2016) but also has cytoplasmic targets including MTs (de Mareuil et al., 2005). To our knowledge, no current research describes the effect of MT inhibitors on Tat-expressing B-cells.

MATERIALS AND METHODS

Cell Lines and Microtubule Inhibitors

Human B-cell [RPMI8866 and Tat-GFP expressing RPMI8866 (RPMI8866-Tat-GFP)] and T-cell (Jurkat) lines were used in the study. Cells were maintained in EX-CELL Medium (SAFC Biosciences, United States) supplemented with L-glutamine and 10% FBS (Paneco, Russia). The effects of three MT inhibitors on cell cycle and cell death were evaluated in the study: paclitaxel (taxol; Sigma, United States), nocodazole (Biochem, United States) and vinorelbine (Sigma, United States). MT inhibitors were added to the medium 24 h prior to analysis at final concentrations of 3; 10; 30; 100; 300; and 1000 nM.

Fluorescence Staining

Propidium iodide for DNA staining: The protocol for cell cycle analysis in suspension cells was published previously (Potashnikova et al., 2018).

Anti-caspase 3 immunostaining kit: PE-conjugated antibodies against active caspase 3 (BD, United States) were used to assess percentages of apoptotic cells. Cell fixation, permeabilization and staining were performed using supplied buffers based on the manufacturer's instructions.

Multi-label cell cycle and apoptosis staining: live cell suspensions of RPMI8866 and RPMI8866-Tat-GFP were simultaneously stained with tetramethyl-rhodamine ethyl ester (TMRE) for membrane potential, Hoechst33342 for DNA and annexin V-Alexa Fluor 647 (all Thermo Fisher Scientific, United States) for phosphatidylserine externalization. RPMI8866 cells were also stained with CellEvent fluorescent caspase 3/7 substrate (Thermo Fisher Scientific, United States): RPMI8866-Tat-GFP cells were not stained with CellEvent to avoid fluorescence signal conflict. The staining protocol was published previously (Vorobjev and Barteneva, 2016).

Flow Cytometry

Cells were analyzed using a FACSaria SORP cell sorter at Ex.407 nm/Em.425–475 nm for Hoechst33342, Ex.488 nm/Em.515–535 nm for CellEvent, Ex.561 nm/Em.575–590 nm for TMRE, PI and anti-caspase3-PE and Ex.640 nm/Em.663–677 nm for annexin V-Alexa Fluor 647. Flow cytometry data were acquired and analyzed using FACS Diva v.6.1.3 software (BD, United States). Each measurement was performed at least in triplicate.

Fluorescence Microscopy

Cell suspensions simultaneously stained with TMRE, Hoechst33342, CellEvent and annexin V-Alexa Fluor 647 were analyzed using a Nikon Ti Eclipse microscope under PlanApo 60×/1.4 objective. Images were recorded by Hamamatsu ORCA FLASH2 digital camera, using the following filter sets: Ex.450–490 nm/Em.510–540 nm; Ex.340–380 nm/Em.435–485 nm; Ex.530–560 nm/Em.573–640 nm and Ex.595–645 nm/Em.665–715 nm.

Statistical Analysis

Data from biological repeats were calculated as mean and standard deviation and plotted in GraphPad Prism software (United States). Unpaired *t*-test (95% confidence interval) was used as significance test.

Electron Microscopy

Cells were fixed in 4% glutaraldehyde (Ted Pella, United States) in 0.1 M Sørensen phosphate buffer for 2 h, post-fixed with 1% osmium tetroxide (Sigma, United States) for 1 h, dehydrated in ethanol and propylene oxide and embedded in Spi-pon 812 epoxy resin (SPI Inc., United States). Ultrathin sections were cut using an LKB III ultramicrotome (LKB), stained with uranyl acetate

and lead citrate, and photographed using a JEM-1400 electron microscope (Jeol, Japan)¹.

RESULTS

The Mitostatic Response to Various MT Inhibitor Concentrations Is Non-linear

We tested the mitostatic effect of three common stabilizing (paclitaxel) and depolymerizing (nocodazole, vinorelbine) MT inhibitors, on RPMI8866, RPMI8866-Tat-GFP (B-lymphocytes) and Jurkat (T-lymphocytes) cell lines. Linear gates were set to determine cell percentages at different cell cycle stages on DNA content curves (Figures 1A–C).

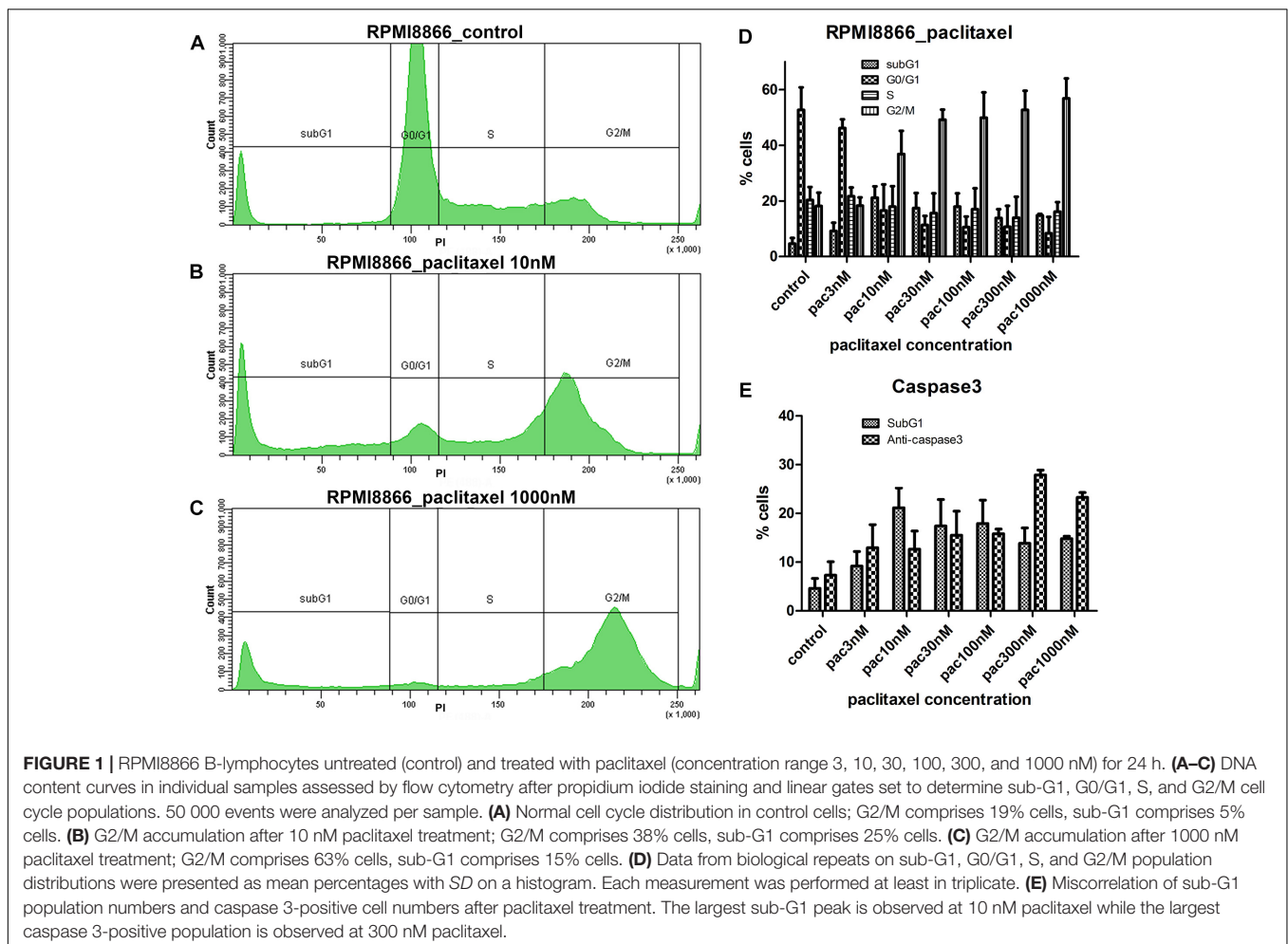
Microtubule inhibitors uniformly prompted cell accumulation in G2/M in a non-linear fashion: we found “trigger” concentrations sufficient to accumulate cells in G2/M phase that fell into 10–100 nM range for all inhibitors and cell lines. Concentrations below the “trigger” retained cell cycle

distribution close to normal. For example, for 3 nM paclitaxel we observed 46% cells in G0/G1, 22% cells in S, and 18% in G2/M for RPMI8866 cells compared to 53% cells in G0/G1, 20% cells in S, and 18% in G2/M in control (Figure 1D). Concentrations above the “trigger” increased the G2/M population peak with a subsequent decrease of the G1 peak (Figures 1B,C and Supplementary Figure S1). Similar response patterns were achieved for every MT inhibitor; however, paclitaxel graphs were chosen as most representative.

The Sub-G1 Population on DNA Content Curves Likely Represents Apoptotic Cells but Its Percentage Does Not Correlate With Percentages of Caspase-3 Positive Cells

The number of cells with sub-G1 DNA content increased significantly in every MT inhibitor concentration compared to untreated control ($p < 0.05$, unpaired t -test) (Figures 1A–C and Supplementary Figure S1). Hypodiploid amounts of DNA can be explained by nucleic acid degradation in late apoptosis. Intriguingly, the largest sub-G1 populations did not correspond

¹For Original Research articles, please note that the Material and Methods section can be placed in any of the following ways: before Results, before Discussion or after Discussion.



to the highest MT inhibitor concentrations. Sub-G1 cell percentages did not significantly differ at “trigger,” sub-“trigger” and high MT inhibitor concentrations. The only significant difference was obtained for paclitaxel: the highest percentage of cells in sub-G1 (21%) was present in 10 nM paclitaxel; that was significantly increased compared to 3, 300, and 1000 nM paclitaxel and insignificantly different from 30 to 100 nM paclitaxel ($p < 0.05$, unpaired t -test). To assess apoptosis levels, cells were immunostained for active caspase 3. Lack of correlation between sub-G1 and caspase 3-positive cell percentages was observed (**Figure 1E**) as the number of caspase 3-positive cells at 10 nM paclitaxel (13%) was similar to the numbers of caspase 3-positive cells in the range of 3–100 nM paclitaxel. To further investigate the apparent contradiction between the results obtained by DNA content analysis and anti-caspase 3 staining a novel protocol for live cell analysis was developed and tested on B-lymphocytes.

Live Cell Staining With Hoechst33342 Provides Similar Results to PI Staining and Allows a Simultaneous Multi-Parameter Apoptosis Assessment

Live cell suspensions of RPMI8866 and RPMI8866-Tat-GFP were simultaneously stained with TMRE, Hoechst33342, CellEvent fluorescent caspase 3/7 substrate and annexin V-Alexa Fluor 647. Combined DNA content and apoptotic marker cell labeling was visualized using flow cytometry and fluorescence microscopy. Hoechst33342-based DNA content analysis provided a dose response pattern similar to PI staining with G2/M peak shift at “trigger” concentrations (**Supplementary Figure S2**). Dying cells exhibit the typical pattern of apoptotic events (Vorobjev and Barteneva, 2015): the gradual TMRE fluorescence decrease corresponding to mitochondrial membrane potential (MMP) loss, CellEvent fluorescence corresponding to caspase 3 activation and annexin V surface staining corresponding to phosphatidylserine externalization (**Figures 2D–I**). This result was confirmed by electron microscopy (**Figures 2J–N**): multiple apoptotic cells were detected in the paclitaxel-treated specimen. Early stages were characterized by chromatin marginalization; at later stages, cell volume decreased markedly, accompanied by cytoplasm condensation. Dead cells had destroyed plasma membranes and cytoplasmic organelles, but inside them the residuals of nuclei were still distinguishable.

Sub-G1 cell accumulation was observed at various rates upon MT inhibitor treatment and was most prominent in 10 nM paclitaxel (26%) (**Figures 2A–C**). The sub-G1 population was heterogeneous and contained cell debris with apoptotic markers and low MMP and cells with no apoptotic markers, hypodiploid DNA content and a two-fold decreased MMP compared to live cells with normal ploidy. Median TMRE fluorescence intensity was 976 a.u. for cell debris, 22380 a.u. for hypodiploid cells and 48265 a.u. for normal live cells (**Figures 2F–G**). Differences were statistically significant ($p < 0.05$). Fluorescence microscopy revealed live cells, apoptotic cells, cell debris and a fraction

of small-sized live cells, often with micronuclei and dim mitochondria, in all MT inhibitor-treated specimens (**Supplementary Figure S3**).

DISCUSSION

It was shown that MT inhibitor concentrations sufficient for cell motility suppression can be lower than those needed for mitotic arrest (Kapoor and Panda, 2012; Molina et al., 2013). One of the thrilling questions is whether cytotoxic effects can be exerted at low concentrations of MT inhibitors. To answer this, we opted for a multi-parameter simultaneous cell cycle and cell death assessment. The proposed approach was derived from the two protocols described previously (Vorobjev and Barteneva, 2016; Potashnikova et al., 2018). It provides an easy and robust way to separately estimate the cytotoxic and mitostatic effects of microtubule inhibitors. The staining is suitable for high-throughput flow cytometry and imaging flow cytometry, as well as for microscopic evaluation of apoptosis kinetics in heterogeneous cell populations after chemotherapeutic treatment.

Using such an approach we described the non-linear dose response to an array of MT inhibitors, which seems to be universal. The “trigger” concentrations fall between 10–30 nM for paclitaxel, 30–100 nM for nocodazole and 10–30 nM for vinorelbine. Increasing dosages do not significantly alter G2/M accumulation. Despite the controversial data on B-cell responses to various types of MT inhibitors (Beswick et al., 2006; Frezzato et al., 2014) in our experiments the pattern of response to all compounds was similar for all cell lines. Our data on cell cycle accumulation and cell death percentages after MT inhibitor treatment correspond to the published data on adherent cells (Di Cesare et al., 2017).

Cells accumulated in G2/M phase die via apoptosis, exhibiting mitochondrial membrane potential (MMP) decrease, caspase activation and phosphatidylserine externalization. A sub-G1 population on DNA content curves includes late apoptotic cells and cell debris. However, at low paclitaxel concentrations this population also includes particularly large numbers of cells with MMP decreased only two-fold compared to normal cells and no markers of apoptosis. This explains the miscorrelation between sub-G1 and caspase 3-positive cell percentages observed in a range of paclitaxel concentrations. Such addition biases the interpretation of sub-G1 population as homogeneous and invariably apoptotic. Sub-G1 cells were described in other cell models as potentially non-viable products of aberrant mitosis (Demidenko et al., 2008) resulting from MT inhibition. Using fluorescence microscopy we visualized cells with smaller nuclei, often with micronuclei, and dim TMRE staining that fit the description of such cells. While their viability has to be further investigated, they present a distinctly different pattern of response to MT inhibitors compared to standard G2/M-accumulating cells that has to be accounted for.

Interestingly, MT inhibitors had the same effect on Tat-expressing B-lymphocytes (**Supplementary Figures S1, S2**).

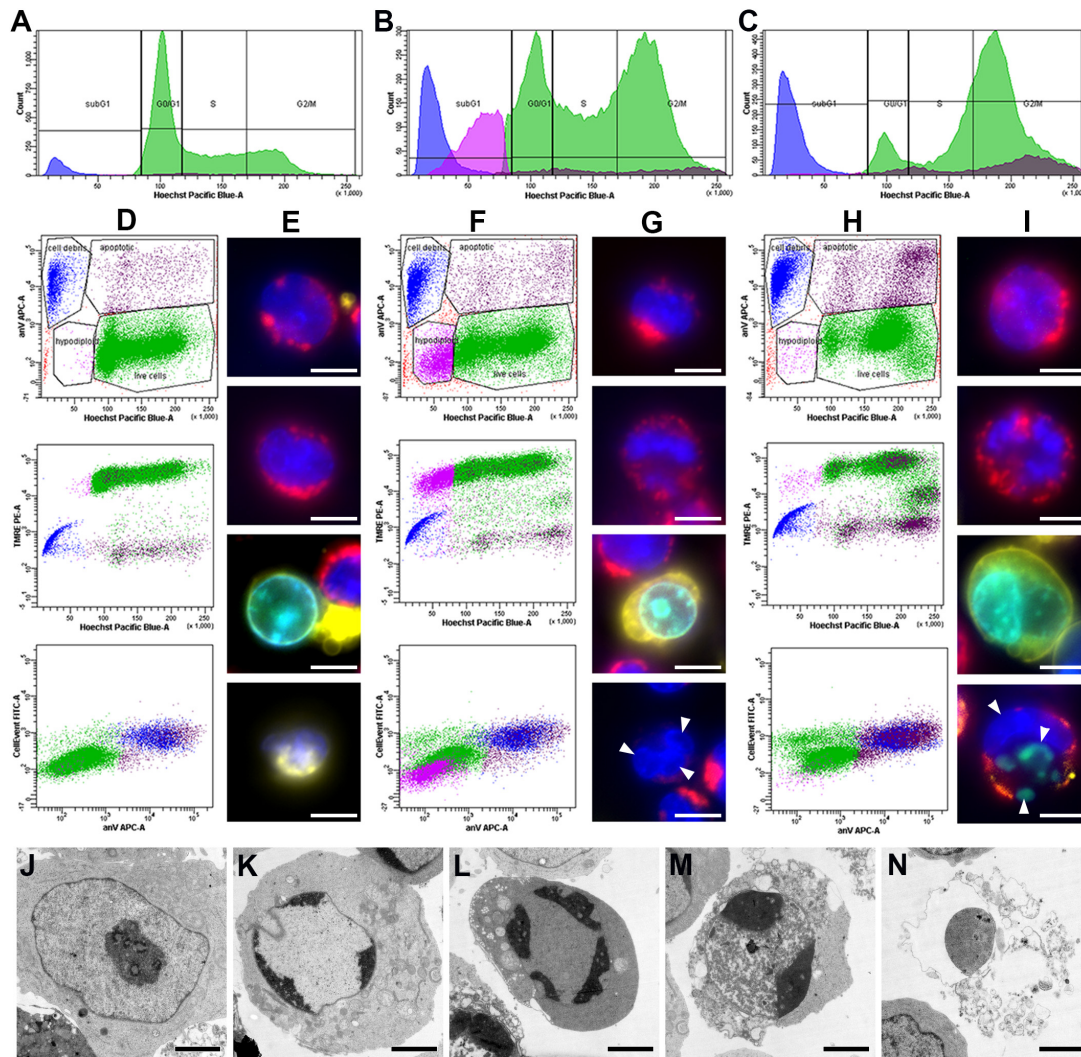


FIGURE 2 | RPMI8866 B-lymphocytes untreated (control) and treated with paclitaxel (10 and 1000 nM) for 24 h. **(A–C)** DNA content curves in individual samples assessed by flow cytometry after Hoechst33342 staining and linear gates set to determine sub-G1, G0/G1, S, and G2/M cell cycle populations [colored subpopulations correspond to live cells (green), apoptotic cells (brown), hypodiploid cells (purple) and cell debris (blue) as gated on dot plots **(D–F)**]. 50 000 events were analyzed per sample. **(A)** Normal cell cycle distribution in control cells; G2/M comprises 18% cells, sub-G1 comprises 6% cells. **(B)** G2/M accumulation after 10 nM paclitaxel treatment; G2/M comprises 30% cells, sub-G1 comprises 26% cells. **(C)** G2/M accumulation after 1000 nM paclitaxel treatment; G2/M comprises 49% cells, sub-G1 comprises 19% cells. **(D,F,H)** Dot plots representing simultaneous staining of RPMI8866 B-lymphocytes with Hoechst33342, TMRE, annexin V-Alexa Fluor 647, and CellEvent. Region gates are set to determine live cells (green), apoptotic cells (brown), hypodiploid cells (purple) and cell debris (blue) based on Hoechst33342 vs. annexin V staining. **(D)** Normal apoptosis rate in control cells. Region gates are set to live cells (green) – 89.4%, apoptotic cells (brown) – 3.2%, hypodiploid cells (purple) – 0.6% and cell debris (blue) – 6.8% based on Hoechst33342 vs. annexin V staining. The colors of the gated populations remain the same in the TMRE vs. Hoechst33342 and CellEvent vs. annexin V graphs. **(F)** G2/M and sub-G1 accumulation after 10 nM paclitaxel treatment. Region gates are set to live cells (green) – 69.0%, apoptotic cells (brown) – 4.9%, hypodiploid cells (purple) – 13.5% and cell debris (blue) – 12.6% based on Hoechst33342 vs. annexin V staining. The colors of the gated populations remain the same in the TMRE vs. Hoechst33342 and CellEvent vs. annexin V graphs. **(H)** G2/M accumulation after 1000 nM paclitaxel treatment. Region gates are set to live cells (green) – 67.0%, apoptotic cells (brown) – 13.3%, hypodiploid cells (purple) – 1.6% and cell debris (blue) – 18.1% based on Hoechst33342 vs. annexin V staining. The colors of the gated populations remain the same in the TMRE vs. Hoechst33342 and CellEvent vs. annexin V graphs. **(E,G,I)** Fluorescence images of cells untreated (control) and treated with paclitaxel (10 and 1000 nM) for 24 h. Simultaneous staining of RPMI8866 B-lymphocytes with Hoechst33342 (blue), TMRE (red), annexin V-Alexa 647 (yellow), and CellEvent (green). Scale bar – 10 μm . **(E)** Control cells; top two images correspond to live cells with bright nuclear Hoechst33342 and mitochondrial TMRE fluorescence, bottom two images correspond to an apoptotic cell with CellEvent staining in the nucleus and surface annexin V and cell debris with a dim nucleus and surface annexin V. **(G)** 10 nM paclitaxel treatment; top two images correspond to live cells with bright nuclear Hoechst33342 and mitochondrial TMRE fluorescence, third image corresponds to an apoptotic cell with CellEvent staining in the nucleus and surface annexin V, bottom image corresponds to aneuploid (hypodiploid) cell with dim mitochondrial TMRE fluorescence and micronuclei. White arrowheads indicate micronuclei. **(I)** 1000 nM paclitaxel treatment; top two images correspond to live cells with bright nuclear Hoechst33342 and mitochondrial TMRE fluorescence, bottom two images correspond to apoptotic cells with CellEvent staining in the nucleus and surface annexin V with/without micronuclei. White arrowheads indicate micronuclei. **(J–N)** Electron microscopy of cells at various stages of apoptosis after 10 nM paclitaxel treatment. Scale bar – 2 μm . **(J)** Normal cell with typical RPMI8866 lymphocyte morphology. **(K)** Chromatin marginalization. **(L)** Decrease of cell volume and condensation of cytoplasm (cell shrinkage). **(M)** Early stage of cell destruction (secondary necrosis). **(N)** Cellular debris inside which the residual chromatin and cytoplasmic organelles can be distinguished.

Despite some evidence of Tat protein interactions with microtubules (de Mareuil et al., 2005) RPMI8866-Tat-GFP cells do not differ from normal RPMI8866 lymphocytes in their MT inhibitor responses. The relevance of our findings for HIV-associated non-Hodgkin's lymphoma model is important for treating such patients.

Thus cell cycle arrest and cell death may be differentially affected by high and low doses of MT inhibitors which has a big therapeutic potential in oncology.

AUTHOR CONTRIBUTIONS

DP and AS conceived and performed the experiments, analyzed the data, and wrote the manuscript. AT performed the experiments and analyzed the data. ES and IV conceived and performed the experiments, analyzed the data, and edited the manuscript.

FUNDING

The project was funded by Russian Science Foundation Grant #18-75-00033.

ACKNOWLEDGMENTS

The authors acknowledge support from the MSU Program of Development (FACSARIA SORP facility).

REFERENCES

- Bates, D., and Eastman, A. (2017). Microtubule destabilising agents: far more than just antimetabolic anticancer drugs. *Br. J. Clin. Pharmacol.* 83, 255–268. doi: 10.1111/bcp.13126
- Bates, D., Feris, E. J., Danilov, A. V., and Eastman, A. (2016). Rapid induction of apoptosis in chronic lymphocytic leukemia cells by the microtubule disrupting agent BNC105. *Cancer Biol. Ther.* 17, 291–299. doi: 10.1080/15384047.2016.1139245
- Bennouna, J., Delord, J.-P., Campone, M., and Nguyen, L. (2008). Vinflunine: a new microtubule inhibitor agent. *Clin. Cancer Res.* 14, 1625–1632. doi: 10.1158/1078-0432.CCR-07-2219
- Beswick, R. W., Ambrose, H. E., and Wagner, S. D. (2006). Nocodazole, a microtubule de-polymerising agent, induces apoptosis of chronic lymphocytic leukaemia cells associated with changes in Bcl-2 phosphorylation and expression. *Leuk. Res.* 30, 427–436.
- Cortes, J., and Vidal, M. (2012). Beyond taxanes: the next generation of microtubule targeting agents. *Breast Cancer Res. Treat.* 133, 821–830. doi: 10.1007/s10549-011-1875-6
- de Mareuil, J., Carre, M., Barbier, P., Campbell, G. R., Lancelot, S., Opi, S., et al. (2005). HIV-1 Tat protein enhances microtubule polymerization. *Retrovirology* 2:5.
- Demidenko, Z. N., Kalurupalle, S., Hanko, C., Lim, C. U., Broude, E., and Blagosklonny, M. V. (2008). Mechanism of G1-like arrest by low concentrations of paclitaxel: next cell cycle p53-dependent arrest with sub G1 DNA content mediated by prolonged mitosis. *Oncogene* 27, 4402–4410. doi: 10.1038/nc.2008.82
- Di Cesare, E., Verrico, A., Miele, A., Guibettini, M., Rovella, P., Coluccia, A., et al. (2017). Mitotic cell death induction by targeting the mitotic spindle with

SUPPLEMENTARY MATERIAL

The Supplementary Material for this article can be found online at: <https://www.frontiersin.org/articles/10.3389/fphar.2019.00436/full#supplementary-material>

FIGURE S1 | Lymphocytes treated with MT inhibitors (concentration range 3, 10, 30, 100, 300, and 1000 nM) for 24 h and stained for DNA content with propidium iodide. Data from biological repeats on sub-G1, G0/G1, S, and G2/M population distributions presented as mean percentages with SD on a histogram. Graphs in columns represent RPMI8866 B-lymphocytes, RPMI8866-Tat-GFP B-lymphocytes and Jurkat T-lymphocytes, respectively. Graphs in rows represent paclitaxel, nocodazole and vinorelbine, respectively. Jurkat cells were previously known to respond to MT inhibitors and were therefore used as control.

FIGURE S2 | Lymphocytes treated with MT inhibitors (concentration range 3, 10, 30, 100, 300, and 1000 nM) for 24 h and stained for DNA content with Hoechst33342. Data from biological repeats on sub-G1, G0/G1, S, and G2/M population distributions presented as mean percentages with SD on a histogram. Graphs in columns represent RPMI8866 B-lymphocytes and RPMI8866-Tat-GFP B-lymphocytes, respectively. Graphs in rows represent paclitaxel, nocodazole and vinorelbine, respectively.

FIGURE S3 | Fluorescence image galleries of RPMI8866 B-lymphocytes treated with a low dose of MT inhibitor 10 nM paclitaxel for 24 h. Simultaneous staining with Hoechst33342 (blue), TMRE (red), annexin V-Alexa 647 (yellow), and CellEvent (green). Scale bar – 10 μ m. **(A)** Live cells with normal morphology have bright round nuclei, bright mitochondrial TMRE fluorescence and bear no apoptotic markers. **(B)** Apoptotic cells have TMRE-negative mitochondria, CellEvent caspase substrate staining co-localized with nuclear staining and surface-bound annexin V indicating phosphatidylserine externalization. **(C)** Cell debris and late apoptotic cells have smaller size, irregular shape, TMRE-negative mitochondria, deformed nuclei, often with CellEvent staining, and surface-bound annexin V indicating phosphatidylserine externalization. **(D)** small-sized cells with small nuclei, micronuclei, few TMRE-dim mitochondria, and no apoptotic markers. White arrowheads indicate micronuclei.

- tubulin-inhibitory indole derivative molecules. *Oncotarget* 8, 19738–19759. doi: 10.18632/oncotarget.14980
- Donehower, R. C., and Rowinsky, E. K. (1993). An overview of experience with TAXOL (paclitaxel) in the U.S.A. *Cancer Treat. Rev.* 19(Suppl. C), 63–78.
- Dumontet, C., and Jordan, M. A. (2010). Microtubule-binding agents: a dynamic field of cancer therapeutics. *Nat. Rev. Drug Discov.* 10, 790–803. doi: 10.1038/nrd3253
- Frezzato, F., Trimarco, V., Martini, V., Gattazzo, C., Ave, E., Visentin, A., et al. (2014). Leukaemic cells from chronic lymphocytic leukaemia patients undergo apoptosis following microtubule depolymerization and Lyn inhibition by nocodazole. *Br. J. Haematol.* 165, 659–672. doi: 10.1111/bjh.12815
- Gopal, S., Patel, M. R., Yanik, E. L., Cole, S. R., Achenbach, C. J., Napravnik, S., et al. (2013). Temporal trends in presentation and survival for HIV-associated lymphoma in the antiretroviral therapy era. *J. Natl. Cancer Inst.* 105, 1221–1229. doi: 10.1093/jnci/djt158
- Grigoriev, I. S., Chernobelskaya, A. A., and Vorobjev, I. A. (1999). Nocodazole, vinblastine and taxol at low concentrations affect fibroblast locomotion and saltatory movements of organelles. *Membr. Cell Biol.* 13, 23–48.
- Jordan, M. A., Toso, R. J., Thrower, D., and Wilson, L. (1993). Mechanism of mitotic block and inhibition of cell proliferation by taxol at low concentrations. *Proc. Natl. Acad. Sci. U.S.A.* 90, 9552–9556.
- Kapoor, S., and Panda, D. (2012). Kinetic stabilization of microtubule dynamics by indanocine perturbs EB1 localization, induces defects in cell polarity and inhibits migration of MDA-MB-231 cells. *Biochem. Pharmacol.* 83, 1495–1506. doi: 10.1016/j.bcp.2012.02.012
- Kaverina, I., and Straube, A. (2011). Regulation of cell migration by dynamic microtubules. *Semin. Cell Dev. Biol.* 22, 968–974. doi: 10.1016/j.semcdb.2011.09.017
- Liao, G., Nagasaki, T., and Gundersen, G. G. (1995). Low concentrations of nocodazole interfere with fibroblast locomotion without significantly affecting

- microtubule level: implications for the role of dynamic microtubules in cell locomotion. *J. Cell Sci.* 108, 3473–3483.
- Molina, A., Velot, L., Ghouinem, L., Abdelkarim, M., Bouchet, B. P., Luissint, A. C., et al. (2013). ATIP3, a novel prognostic marker of breast cancer patient survival, limits cancer cell migration and slows metastatic progression by regulating microtubule dynamics. *Cancer Res.* 73, 2905–2915. doi: 10.1158/0008-5472.CAN-12-3565
- Musunova, Y. R., Sheval, E. V., Dib, C., Germini, D., and Vassetzky, Y. S. (2016). Functional roles of HIV-1 tat protein in the nucleus. *Cell. Mol. Life Sci.* 73, 589–601. doi: 10.1007/s00018-015-2077-x
- Perez, E. A. (2009). Microtubule inhibitors: differentiating tubulin-inhibiting agents based on mechanisms of action, clinical activity, and resistance. *Mol. Cancer Ther.* 8, 2086–2095. doi: 10.1158/1535-7163.MCT-09-0366
- Potashnikova, D., Golyshev, S., Penin, A., Logacheva, M., Klepikova, A., Zharikova, A., et al. (2018). FACS isolation of viable cells in different cell cycle stages from asynchronous culture for RNA sequencing. *Methods Mol. Biol.* 1745, 315–335. doi: 10.1007/978-1-4939-7680-5_18
- Sève, P., Reiman, T., Isaac, S., Trillet-Lenoir, V., Lafanéchère, L., Sawyer, M., et al. (2008). Protein abundance of class III beta-tubulin but not Delta2-alpha-tubulin or tau is related to paclitaxel response in carcinomas of unknown primary site. *Anticancer Res.* 28, 1161–1167.
- Vendrame, E., Hussain, S. K., Breen, E. C., Magpantay, L. I., Widney, D. P., Jacobson, L. P., et al. (2014). Serum levels of cytokines and biomarkers for inflammation and immune activation, and HIV-associated non-Hodgkin B-cell lymphoma risk. *Cancer Epidemiol. Biomarkers Prev.* 23, 343–349. doi: 10.1158/1055-9965.EPI-13-0714
- Vorobjev, I., and Barteneva, N. (2016). Temporal heterogeneity in apoptosis determined by imaging flow cytometry. *Methods Mol. Biol.* 1389, 221–233. doi: 10.1007/978-1-4939-3302-0_16
- Vorobjev, I., and Barteneva, N. S. (2015). Temporal heterogeneity metrics in apoptosis induced by anticancer drugs. *J. Histochem. Cytochem.* 63, 494–510. doi: 10.1369/0022155415583534
- Windebank, A. J. (1999). Chemotherapeutic neuropathy. *Curr. Opin. Neurol.* 12, 565–571.
- Xie, X., Wu, Y., Luo, S., Yang, H., Li, L., Zhou, S., et al. (2017). Efficacy and toxicity of low-dose versus conventional-dose chemotherapy for malignant tumors: a meta-analysis of 6 randomized controlled trials. *Asian Pac. J. Cancer Prev.* 18, 479–484.
- Yang, H., Ganguly, A., and Cabral, F. (2010). Inhibition of cell migration and cell division correlates with distinct effects of microtubule inhibiting drugs. *J. Biol. Chem.* 285, 32242–32250. doi: 10.1074/jbc.M110.160820

Conflict of Interest Statement: The authors declare that the research was conducted in the absence of any commercial or financial relationships that could be construed as a potential conflict of interest.

Copyright © 2019 Potashnikova, Saidova, Tvorogova, Sheval and Vorobjev. This is an open-access article distributed under the terms of the Creative Commons Attribution License (CC BY). The use, distribution or reproduction in other forums is permitted, provided the original author(s) and the copyright owner(s) are credited and that the original publication in this journal is cited, in accordance with accepted academic practice. No use, distribution or reproduction is permitted which does not comply with these terms.